2021 43rd Annual International Conference of the
IEEE Engineering in Medicine & Biology Society (EMBC)
Oct 31 - Nov 4, 2021. Virtual Conference

# Design of a System for Magnetic-Resonance-Guided Irreversible Electroporation

Joris Hubmann[1], Thomas Gerlach[1], Enrico Pannicke[1],
Bennet Hensen[2], Frank Wacker[2], Oliver Speck[3] and Ralf Vick[1]

***Abstract*— Irreversible electroporation (IRE) is a non-thermal tumor ablation method where strong electrical fields between at least two electrodes are used and can be seen as an alternative to thermal ablation techniques. The therapy outcome directly dependents on the position of the electrodes. Real-time monitoring of the IRE by magnetic resonance imaging (MRI) would allow to detect unwanted electrode displacement and to apply visualization methods for the ablation area. This requires that the IRE generator does not significantly interfere with the MRI. Currently, there is no IRE generator available designed for MRI-guided IRE.**
**This paper presents an IRE system specifically developed for use in an MRI environment. The system is initially tested with a standard IRE sequence and then the interference between a clinical 3 T MRI device and the IRE system is investigated using a noise measurement and the signal-to-noise ratio (SNR) of images acquired with a gradient echo (GRE) sequence. The results show, that although the SNR of the images decrease by maximal 36 % when the IRE system is switched on, image quality does not visibly degrade. Hence, MRI-guided IRE is feasible with the proposed system.**

***Clinical relevance*— This paper demonstrates the possibility of MRI-guided IRE with only minor image degradation when the IRE system is used in parallel with MRI imaging.**

## I. INTRODUCTION

Minimally invasive percutaneous ablation therapies offer the possibility of patient gentle treatment of tumors that are difficult to access [1]. In contrast to radiofrequency and microwave ablation, irreversible electroporation (IRE) is a nonthermal ablation technique [2]. Instead, it uses strong pulsed electrical fields to create artificial pores within the cell membranes of the tissue. Thereby, IRE has the advantage over other ablation methods of sharp ablation edges, sparing connective tissue and having no heat sink effect, which makes it feasible for tumors within well perfused areas [2], [3]. The electrical field threshold necessary for IRE varies between $300\,\mathrm{V\,cm^{-1}}$ and $1500\,\mathrm{V\,cm^{-1}}$. Thereby, it is dependent on the tissue type and the ablation parameters such as the pulse duration and the number of pulses [4].

For an IRE ablation, multiple electrodes are inserted in the region of the tumor and a sequence of electrical pulses is applied to the electrodes to generate the intended electrical field within the tumor [5].

In order to ablate the whole tumor, electrode placement is crucial. In the clinical routine, a planning software is used to determine the optimal electrode placement for each specific tumor. Additionally, external forces due to body movement, stress on the cables or the electric current can change the electrode position, hence, the ablation area. To assist the electrode placement and to check the electrode position after insertion, medical imaging technologies like computer tomography, ultrasound, and magnetic resonance imaging (MRI) are used [5]. With real time imaging of the IRE process the ablation performance can be further increased. Due to its high soft tissue contrast, no radiation, and the possibility of arbitrary slice selection the MRI can be used to monitor the electrode placement [6]. Additionally, MRI offers the possibility of current density imaging (CDI), which can be used to monitor the ablation area in-vivo [7].

The MRI uses frequency information to obtain images. Therefore, to preserve good image quality, it is necessary to keep the electrical interference between the MRI and external electric devices as low as possible [8].

Because there is no IRE system available specifically designed for use within an MRI environment, this work proposes an IRE system to specifically meet the challenges of working in an MRI environment. Furthermore, the system is tested using clinical IRE ablation sequences and its interference with a 3 T Siemens Skyra MRI scanner is examined.

## II. IRE SYSTEM DESIGN

An IRE system must be capable of providing the IRE sequences. These sequences consist of multiple high voltage pulses, which are applied to the cancerous tissue. In the past, many different pulse sequences were developed. In the clinical routine, mostly 70 to 90 pulses with a pulse duration of $70\,\mu\mathrm{s}$ to $100\,\mu\mathrm{s}$ are used. Thereby, the pause between the pulses is either heart rate triggered or in the range of $1\,\mathrm{s}$ [5]. The voltages applied to the electrodes vary according to the ablated tissue between $450\,\mathrm{V}$ and $3000\,\mathrm{V}$. Whereby most sequences do not exceed $2000\,\mathrm{V}$ [5]. Due to these voltages between the electrodes and the conductivity of the tissue, currents up to $50\,\mathrm{A}$ can occur when performing an IRE ablation.

The proposed IRE system is a first prototype and can provide a maximum voltage of $2000\,\mathrm{V}$, unipolar, rectangular pulses, with a width between $20\,\mu\mathrm{s}$ to $160\,\mu\mathrm{s}$ and a current

[1] Joris Hubmann, Thomas Gerlach, Enrico Pannicke and Ralf Vick are with the Faculty of Electrical Engineering and Information Technology, Otto-von-Guericke University, Universitätspl. 2, 39106 Magdeburg, Germany hubmannjoris@yahoo.de

[2] Bennet Hensen and Frank Wacker are with the Department of Radiology, Hannover Medical School, 30625 Hanover, Germany

[3] Oliver Speck is with the Faculty of Natural Science, Department of Physics, Otto-von-Guericke University, Universitätspl. 2, 39106 Magdeburg, Germany

978-1-7281-1178-0/21/$31.00 ©2021 IEEE

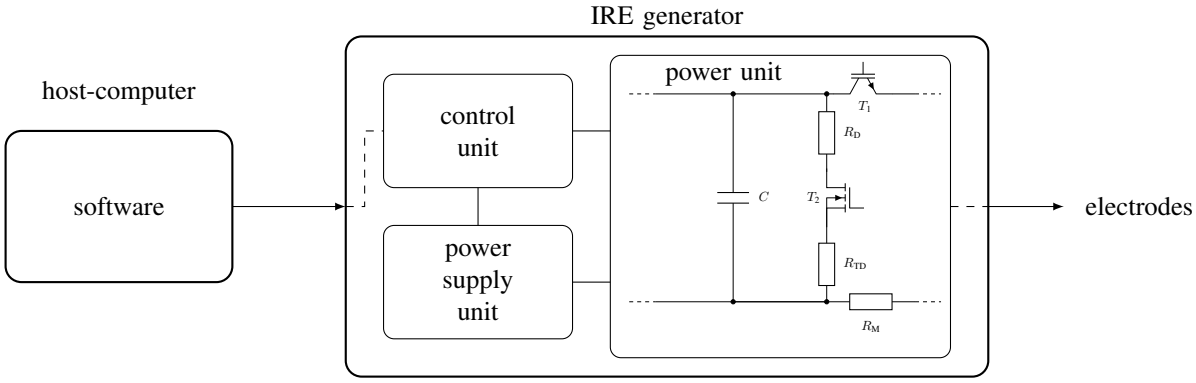


Fig. 1: System architecture of the IRE system

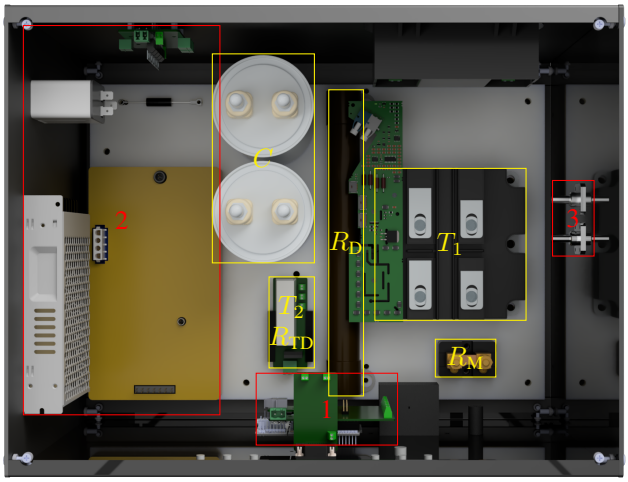


Fig. 2: IRE system prototype (without wires) with 1: control unit, 2: power supply unit, 3: electrode wire connection and the rest being the power unit (yellow)

carrying capacity of more than 50 A. The minimal requirements for the IRE system are outlined in Tab. I.

A schematic representation of the IRE system is shown in Fig. 1. The system is based on two main units. A host-computer and an IRE generator. From the host-computer the software allows the user to set the ablation parameters. The IRE generator receives the parameters and is divided into 3 subunits. A control unit, which is the communication interface of the generator, a supply unit to provide the required voltages and a power unit that delivers the high voltage pulses to the electrodes.

TABLE I: IRE system minimum requirements

| Requirement aspect | Requirement |
|---|---|
| output voltage | 2000 V |
| current capacity | 50 A |
| pulse duration | 70 µs to 100 µs |
| pulse form | rectangular, unipolar |

The power supply unit contains two switching power supplies and multiple linear regulators to generate the voltages necessary for the generator. One switching power supply (HP 4C24-P250-I5, HVP GmbH, Germany) provides the high voltages for the ablation and the other one (LRS-150-24, MEAN WELL, China) is used to generate a DC voltage out of the line voltage. The linear regulators provide the voltages needed for powering the control unit and other supplementary circuitry.

The control unit uses the information sent by the host computer to control the high voltage power supply and the transistors $T_1$ (CM600HG-90H, Mitsubishi Electric Corporation, Japan) and $T_2$ (IXTH02N250, IXYS Corporation, USA).

The power unit applies the high voltage to the tissue. Hereby, the capacitor bank $C$ (C20AZGR5220AASK, KEMET Electronics Corporation, USA) is charged initially by the high voltage power supply of the power supply unit. After the charging process, the high voltage power supply is disabled and the ablation sequence is generated through switching the transistor $T_1$. After the ablation process is finished, the capacitor bank is discharged through the resistor $R_D$ (L225J20KE, Ohmite Manufacturing Company, USA) due to safety reasons by driving the transistor $T_2$. The prototype with its components is displayed in Fig. 2.

To address the MRI compatibility only one transistor is used to generate the IRE sequences and linear regulators are implemented to reduce the generated switching noise. Additionally, the generator is housed within an aluminum casing to reduce emitted radio frequency noise.

For user safety, all components which have a connection to the outside of the casing are either galvanically isolated from the high voltage or designed in a way, that they are not touchable. Additionally, the casing is connected to protective earth.

## III. METHODS

The designed IRE system must be tested under clinical conditions to guarantee a proper functionality. In order to

evaluate the MRI compatibility, the interaction between the IRE system and the MRI must be analyzed.

### A. System Test

The IRE system functionality is checked using an IRE sequence previously studied by Trimmer et al. [10]. Therefore, the ablation sequence is set to 70 pulses at 2000 V with a pulse duration of 100 µs and between each pulse there is a pause of 1 s. A phantom consisting of water (1000 ml), hydroxyethyl cellulose (HEC, 31 g l$^{-1}$), salt (10.8 g l$^{-1}$) and 1 ml of contrast agent (gadoteric acid Dotarem, Guerbet S.A., France) with a conductivity of 20.5 mS cm$^{-1}$ is used and is thereby replacing human tissue [11]. The electrodes are inserted into the HEC phantom with a distance of 1 cm from each other and connected to the IRE system via coaxial cables. The IRE sequence is applied to the HEC phantom and the output voltage and current is measured via an oscilloscope at VM and IM.

### B. IRE - MRI interference: noise spectra

To keep radiated emissions at a minimum the generator is placed in the control room outside of the MRI shielding cabin and connected to the electrodes via coaxial cables through a wave guide. The electrodes are inserted into a HEC phantom and both are placed within the isocenter of a Siemens 3 T Skyra MRI. With the MRI three cases are examined:

- case 1: IRE system off
- case 2: IRE system in stand-by
- case 3: Ablation

For these three cases the scanner's proprietary noise spectra sequence is applied to determine the emitted noise by the IRE system. This sequence measures the noise around the larmor frequency of 123.259 951 MHz with an effective bandwidth of 500 kHz and a total bandwidth of 1 MHz. To acquire the noise a coil array of four coils is used. The sequence parameters are depicted in Tab. IIa. The results of the measurements are evaluated and examined with respect to the influence of the IRE system on the noise.

TABLE II: MRI Sequence parameters of the noise spectra measurement (a) and the gradient echo sequence (b)

(a) noise spectra

| Parameter | Value |
|---|---|
| TR | 20 ms |
| averages | 50 |
| measurements | 30 |
| coils | 4 (flex) |
| eff. bandwidth | 500 kHz |

(b) gradient echo

| Parameter | Value |
|---|---|
| FoV read | 150 mm |
| FoV phase | 100 % |
| slice thickness | 5 mm |
| TR | 20 ms |
| TE | 7 ms |
| averages | 1 |
| coils | 4 (flex) |
| flip angle | 18° |
| measurements | 20 |
| base resolution | 128 Px |
| image bandwidth | 25 575 Hz |

### C. IRE - MRI interference: images

To further evaluate the interference between the IRE system and the MRI device images with a gradient echo (GRE) sequence are acquired. The test setup is the exact same as for the noise measurement, but instead of the MRI noise sequence, the GRE sequence is used. The parameters of this sequence are depicted in Tab. IIb.

With the GRE sequence the creation of artifacts in the MRI image due to the IRE system is investigated. Furthermore, the signal-to-noise ratio (SNR) and its standard deviation are evaluated as a measure for image quality. According to the corresponding standard for the SNR of medical images, the SNR is calculated by

$$SNR = \frac{\mu}{\sigma}. \tag{1}$$

Hereby, $\sigma$ is the standard deviation of the background and $\mu$ is defined as the average of the signal [9]. The SNR is calculated for each of the 20 measurements performed for the three cases and the sagittal, transversal, and coronal images of the HEC phantom. The mean SNR from the 20 measurements and its standard deviation are then computed for each individual image.

## IV. RESULTS

### A. System Test

Fig. 4 shows the result of the system test. It can be seen that the IRE generator produces the 70 pulses that were set prior to the ablation. But the output voltage varies between 2000 V and 1960 V over the course of the ablation. Besides these variations, the output voltage does not drop during the IRE sequence. The delivered pulses had a spacing of 1 s and the pulse duration is 100 µs. Fig. 5 depicts one of the 70 pulses as a close up. In red the output voltage is displayed showing the 2000 V output voltage are reached after 2.4 µs. During the plateau there is a decrease in output voltage of 7 %. Then after the intended 100 µs the output voltage decreases to 0 V within 5 µs. The output current is displayed in blue. It has an initial peak of 106 A reaching a plateau of 50 A for the duration of the pulse. On the falling edge of the pulse there is an initial peak of −146 A followed by a decaying oscillation with a frequency of 500 kHz which is abated after 17 µs.

### B. IRE - MRI interference: noise spectra

In Fig. 6 the noise spectra of the previously mentioned cases (IRE system off, IRE system in stand-by, Ablation) are depicted. It can be seen that the IRE system only increases the general noise level marginally when in stand-by. Although, there are additional peaks visible for case 2 as well as for case 3. For imaging only the effective bandwidth is pertinent. Therefore, only the noise within the range of ±250 kHz around the center frequency is relevant. Here two main peaks appear for case 2 and case 3 compared to case 1 and hence, are induced by the IRE system. The peak with the mark A in Fig. 6 has a repetition frequency of 500 kHz, whereby the peak with the mark B has no visible

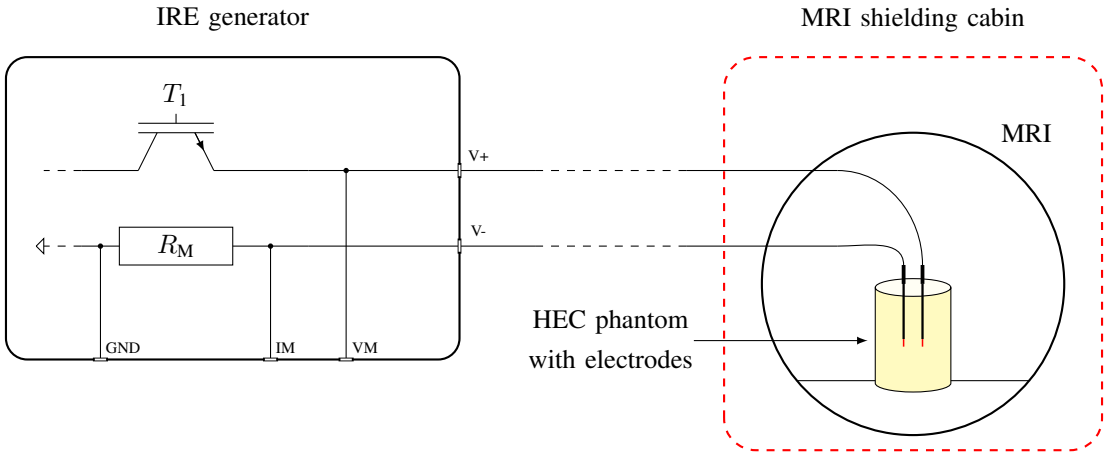


Fig. 3: Test set-up for the interference measurements

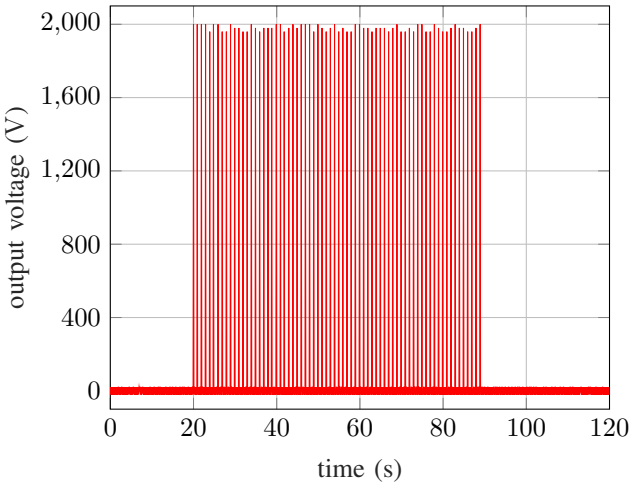


Fig. 4: Output voltage of the IRE generator for 70 pulses at 100 µs and 2000 V

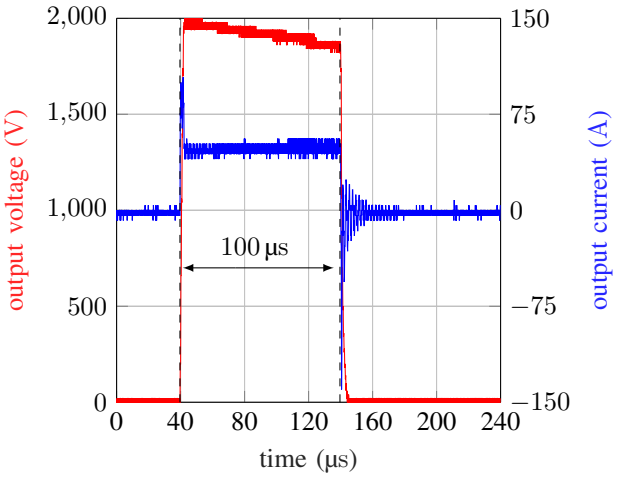


Fig. 5: Output voltage (red) and output current (blue) of the IRE generator for a single pulse out of the pulse set

repetition frequency and is higher but more narrow than peak A. Additionally, there is a third IRE system induced set of peaks which has a repetition frequency of 40 kHz.

### C. IRE - MRI interference: images

The images acquired with the GRE sequence are depicted in Fig. 7 with equal scaling for all images. It is shown, that there are no visible artifacts due to the interference with the IRE system. Nevertheless, the SNR decreases from case 1 to case 2 by 33.8 % for the sagittal, 33.2 % for the coronal and 36.1 % for the transversal view. Between case 2 and case 3 there is only a minor difference in SNR for all three views. But, despite the loss of SNR, no degradation of image quality is noticeable. The SNR standard deviation for case 1 is between 5.4 and 3.9. For case 2 it decreases and lies between 2.2 and 1.6. In case 3 it increases again and reaches values between 5.6 and 3.2. The darker area in Fig. 7g-i is due to gases generated during the ablation sequence as a result of arcing.

## V. DISCUSSION

The system test shows that the IRE system is capable of producing IRE sequences. The voltage drop during a single pulse because of the capacitor discharge can be compensated by either a higher initial voltage or bigger capacitors. For this measurement, the output current was set to the highest current expected to occur within the tissue. Therefore, for most human tissue types the voltage drop will be less. The oscillations on the current are mainly due to the noise generated by the switching power supplies and the big output capacitance of the transistor $T_1$.

Despite the actions taken to reduce the noise of the IRE system, the noise level increases when it is in stand-by or active due to electrical interference between the IRE generator and the MRI scanner. Specifically, a 500 kHz oscillation, which is also visible on the performed system test, is generated by the IRE system and is produced by one of the switching power supplies. In the images acquired with the GRE sequence the additional noise is represented by the reduction in SNR. Although the additional peaks do

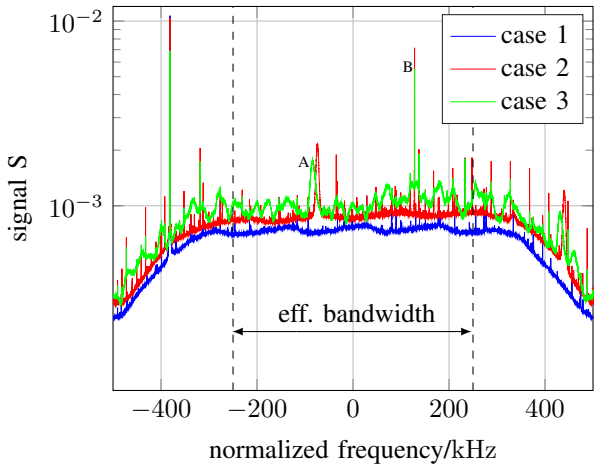


Fig. 6: Noise spectra of the three cases, case 1: IRE system switched off, case 2: IRE system on stand-by, case 3: during IRE ablation

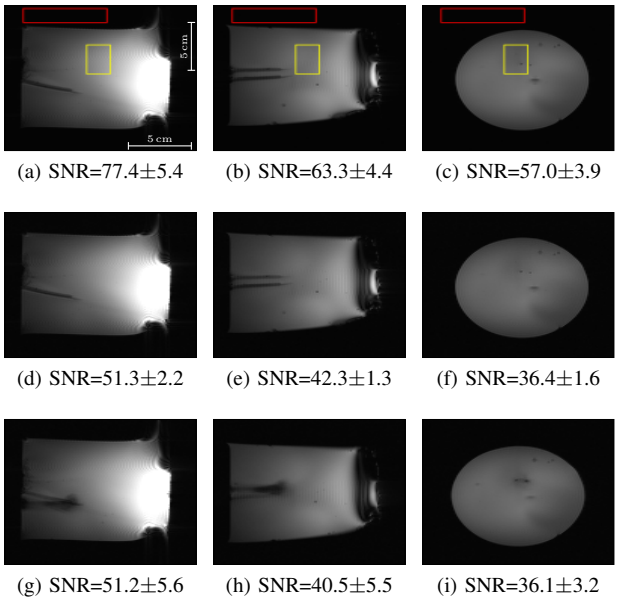


(a) SNR=77.4±5.4 (b) SNR=63.3±4.4 (c) SNR=57.0±3.9

(d) SNR=51.3±2.2 (e) SNR=42.3±1.3 (f) SNR=36.4±1.6

(g) SNR=51.2±5.6 (h) SNR=40.5±5.5 (i) SNR=36.1±3.2

Fig. 7: Images acquired with the GRE sequence for case 1 (a-c), case 2 (d-f) and case 3 (g-i) identically scaled; red rectangle: used background, yellow rectangle: used foreground for the SNR calculation

not generate any artifacts and the image quality is not visibly degraded. The increase in SNR standard deviation between case 2 and case 3 is due to the IRE pulses. The reason for the absence of a visible image quality deterioration is the generally high SNR of the system and the averaging. However, for scanners with less general SNR or other sequences and less averaging the degradation could be visible. Therefore, the effect on image quality of other sequences and other scanners with lower field strength must be evaluated within further research. Specifically, the effect on CDI must be examined, since it provides the possibility of real time supervision of the ablation area.

## VI. CONCLUSIONS

The results of the measurements presented within this work show, that the developed IRE system still produces noise, however, imaging is possible without any further actions and sufficient quality. Hence, the proposed device is capable of performing MRI-guided IRE ablation. Therefore, with the results of this work and in coherence with the research of Kranjc et al. [7] on CDI, MR-guided IRE has great potential and further research is advised.

## ACKNOWLEDGMENT

This work was supported by the Federal Ministry of Education and Research (BMBF), as part of the Magdeburg Research Campus STIMULATE (project no. 13GW0473A).

## REFERENCES

[1] G. S. Gazelle, S. N. Goldberg, L. Solbiati, T. Livraghu, Tumor Ablation with Radio-frequency Energy, Radiology, vol. 217, no. 3, pp. 633-646, 2000.

[2] C. R. Tracy, W. Kabbani, J. A. Cadeddu, Irreversible Electroporation (IRE): A Novel Method for Renal Tissue Ablation, *BJU International*, vol. 107, no. 12, pp. 1982-1987, 2010.

[3] G. Onik, P. Mikus, B. Rubinsky, Irreversible Electroporation: Implications for Prostate Ablation, Technology in Cancer Research & Treatment, vol. 6, no. 4, pp. 295-300, 2007.

[4] C. Jiang, R. V. Davalos, J. C. Bischof, Membrane-Targeting Approaches for Enhanced Cancer Cell Destruction with Irreversible Electroporation, Annals of Biomedical Engineering, vol. 42, no. 1, pp. 193-204, 2014.

[5] K. N. Aycock, R. V. Davalos, Irreversible Electroporation: Background, Theory, and Review of Recent Developments in Clinical Oncology, Bioelectricity, vol. 1, no. 4 pp. 214-234, 2019.

[6] A. j. Sim, E. Kaza, L. Singer, S. A. Rosenberg, A Review of the Role of MRI in Diagnosis and Treatment of Early Stage Lung Cancer, Clinical and Translational Radiation Oncology, vol. 24, pp. 16-22, 2020.

[7] M. Kranjc, S. Kranjc, F. Bajd, G. Sersa, I. Sersa, D. Miklavcic, Predicting Irreversible Electroporation-induced Tissue Damage by Means of Magnetic Resonance Electrical Impedance Tomography, Scientific Reports, vol. 7, no. 10323, pp. 1-10, 2017.

[8] A. Lu, D. A. Woodrum, J. P. Felmlee, C. P. Favazza, K. R. Gorny, Improved MR-thermometry During Hepatic Microwave Ablation by Correcting for Intermittent Electromagnetic Interference Artifacts, Physica Medica, vol. 71, pp. 100-107, 2020.

[9] IEC 62464-1:2018, Magnetic Resonance Equipment for Medical Imaging - Part 1: Determination of Essential Image Quality Parameters.

[10] C. K. Trimmer, A. Khosla, M. Morgan, S. L. Steohenson, A. Ozayar, J. A. Cadeddu, Minimally Invasive Percutaneous Treatment of Small Renal Tumors with Irreversible Electroporation: A Single-Center Experience, Journal of Vascular and interventional Radiology, vol. 26, no. 10, pp. 1465-1471, 2015.

[11] American Society for Testing and Materials, Standard Test Method for Measurement of Radio Frequency Induced Heating On or Near Passive Implants During Magnetic Resonance Imaging, vol. 11.040.40, no. F2182, 2019.